International Journal of Pharmaceutics 395 (2010) 182–197

Contents lists available at ScienceDirect

International Journal of Pharmaceutics

journal homepage: www.elsevier.com/locate/ijpharm

Application of PAMPA-models to predict BBB permeability including efflux ratio, plasma protein binding and physicochemical parameters

Jurgen Mensch[a,*], Libuse Jaroskova L[b], Wendy Sanderson[b], Anouche Melis[c], Claire Mackie[c], Geert Verreck[a], Marcus E. Brewster[a], Patrick Augustijns[d]

[a] ChemPharm Development, Johnson & Johnson Pharmaceutical Research & Development, a division of Janssen Pharmaceutica N.V., 2340 Beerse, Belgium
[b] Bioinformatic Modelling Department, European Discovery Capabilities, Johnson & Johnson Pharmaceutical Research & Development, a division of Janssen Pharmaceutica N.V., Beerse, Belgium
[c] ADME-Tox, Johnson & Johnson Pharmaceutical Research & Development, a division of Janssen Pharmaceutica N.V., Beerse, Belgium
[d] Laboratory for Pharmacotechnology and Biopharmacy, Catholic University of Leuven, O&N Gasthuisberg, Leuven, Belgium

ARTICLE INFO

Article history:
Received 15 December 2009
Received in revised form 20 May 2010
Accepted 21 May 2010
Available online 1 June 2010

Keywords:
Permeability
Solubility
PAMPA
Caco-2
Efflux-ratio
LogBB
Blood–brain barrier
Plasma protein binding

ABSTRACT

This study examines whether algorithms to predict brain penetration of 88 drug candidates could benefit from inclusion of PAMPA data such as P_{eff}, flux and membrane retention. Specifically the ability to fit experimentally derived LogBB data with PAMPA information and compound related physicochemical and structural parameters was assessed. Collected data were analyzed by partial least square analysis and various regression models for LogBB. Four PAMPA methodologies were evaluated in this study including: (1) a PAMPA-BLM (black lipid membrane) model, (2) a PAMPA-DS (double sink) model, (3) a PAMPA-BBB (blood–brain barrier) model and (4) a PAMPA-BBB-UWL (unstirred water layer). Additionally, plasma protein binding (PPB) experiments and a Caco-2 assay were performed to determine the unbound fraction in plasma and the efflux ratio, respectively, for subsets of the selected compounds. This information was combined with the obtained PAMPA data in an effort to improve the predictions of LogBB. Taken in aggregate, the results presented, suggest that the PAMPA-BLM parameters are the most important contributors to predict the LogBB. The optimized multiple linear regression (MLR) relationship including the PAMPA-BLM properties demonstrated a slightly improved prediction compared to the model without the PAMPA-BLM parameters. Including the plasma protein binding of 15 compounds resulted in a significantly improved PAMPA-BLM prediction of LogBB, while integrating the efflux ratio with PAMPA-BLM or PAMPA-BBB P_{eff} values, resulted in improved classification of brain permeable [BBB + (LogBB ≥ 0)] and impermeable [BBB − (LogBB < 0)] compounds.

1. Introduction

The blood–brain barrier (BBB) separates the interstitial fluid (ISF) of the central nervous system (CNS) from the blood. The main component of the blood–brain barrier is the brain endothelium (Abbott et al., 2006; Reese and Karnovsky, 1967; Brightman and Reese, 1969), which manifests a physical and a biochemical component (efflux and metabolism) for the transport of drugs into the CNS. The physical barrier is the result of tight junctions between adjacent endothelial cells, which are approximately 50–100 times tighter than those associated with the peripheral endothelium, meaning that penetration across the endothelium is effectively confined to transcellular mechanisms (Abbott, 2002, 2005). The metabolic barrier is provided by several enzymes which are capable of metabolizing drugs and nutrients (Brownson et al., 1994). The presence of various influx/efflux transporters regulates transcellular traffic facilitating the entry of required nutrients and/or preventing ingress of potentially harmful compounds (Begley and Brightman, 2003; Krämer et al., 2001; Bentz et al., 2005; Cisternino et al., 2004).

In the CNS drug development, it is important that the compounds are able to cross the blood–brain barrier (BBB). Conversely, peripherally acting drugs must show limited ability to cross the BBB to avoid unwanted CNS side effects (Ecker and Noe, 2006). The uptake of a CNS drug candidate from the blood into the brain can be correlated with many physicochemical factors, including lipophilicity, total polar surface area (TPSA), charge state, molecular size, molecular flexibility and number of rotatable bonds as well as hydrogen-bonding potential (Hitchcock and Pennington, 2006; Abraham, 2004; Lipinski, 2004; Clark, 1999; van de Waterbeemd et al., 1998). Further confounding factors include plasma protein binding (PPB), active uptake into the CNS and efflux out of the CNS

* Corresponding author. Tel.: +32 14 606320; fax: +32 14 605838.
E-mail address: jmensch@its.jnj.com (J. Mensch).

0378-5173/$ – see front matter © 2010 Elsevier B.V. All rights reserved.
doi:10.1016/j.ijpharm.2010.05.037

(Jeffrey and Summerfield, 2007; Hammarlund-Udenaes et al., 2008; Maurer et al., 2005; Summerfield et al., 2006; Pardridge, 1995). In this context, a need exists for qualified and validated BBB models suitable to estimate BBB permeability for investigational drugs and further for the application of these models to guide candidate selection in drug discovery.

Developments in combinatorial chemistry have resulted in an increasing number of compounds to test in early discovery meaning that traditional low-throughput in-vivo and in-vitro measurements are inappropriate. For this reason, there has been an increasing interest in in-silico and high throughput in-vitro methods for predicting various in-vivo properties early in the drug discovery process. Although many LogBB models have been developed, the number of compounds used to train LogBB models is limited (Abraham and Hersey, 2006a; Abraham et al., 2006b). The available LogBB data are not only few in number but have also been generated based on different experimental protocols (van de Waterbeemd and Gifford, 2003) and are therefore often uncertain and contradictory.

A promising technology to meet the needs of CNS drug discovery is the parallel artificial permeability assay (PAMPA) first developed as a surrogate for gastrointestinal (GI) absorption. This model is used in pharmaceutical industry to determine the absorption potential of a compound early in the drug discovery and development cycle (Kansy et al., 1998; Masungi et al., 2008; Avdeef, 2003a,b; Brewster et al., 2007; Avdeef, 2005; Kerns et al., 2004; Sugano et al., 2002). PAMPA involves a non-biological artificial membrane and thus only focuses on the prediction of passive transcellular drug absorption. By modifying the lipid composition of the artificial membranes, the system appears capable of identifying compounds as either BBB permeable (BBB+) or non-permeable (BBB−) with reasonable accuracy (Di et al., 2003; Mensch et al., 2010).

In the present study, 88 chemically diverse drug candidates with experimentally determined LogBB values were selected for assessing the permeability values at pH 7.4 with four PAMPA models as previously described by Mensch et al. (2010), in order to predict in-vivo LogBB values. The models applied in this study include: (1) a PAMPA-BLM model using a black lipid membrane and an 18 h incubation period; (2) a PAMPA-DS (double sink) model with a gastrointestinal tract (GIT) lipid membrane and a 4 h incubation period; (3) a PAMPA-BBB method with a porcine polar-brain lipid (PBL) with an 18 h incubation period and (4) a PAMPA-BBB-UWL method with a porcine PBL, an unstirred water layer of 60 μm and a 1 h incubation period. Additionally, physicochemical properties of the selected compounds were calculated (Pipeline Pilot, Accelrys) as well as more complex structural (2D, 3D) properties (MOE, Chemical Computing Group). In an integrated approach, the calculated data as well as the experimentally determined PAMPA data were statistically analyzed using the SimcaP + 12 software (U metrics) to predict the brain penetration (LogBB) via partial least square analysis (PLS). This methodology allows assessing whether prediction of brain penetration (LogBB) can benefit from inclusion of experimental PAMPA results, and if so, which PAMPA model contributes most significantly. Besides the PLS analysis, a multiple regression analysis with backward stepwise selection has been performed on the physicochemical parameters and the PAMPA results of the test set.

Although not all P-gp substrates are excluded from the brain (Summerfield et al., 2006), in-vitro efflux assays can help to explain poor CNS penetration. Therefore, a bidirectional Caco-2 assay was performed on 27 of the selected compounds to determine the efflux ratio (Masungi et al., 2008; Avdeef, 2003a; Mensch et al., 2010). In order to compensate for differences in plasma protein binding, this parameter was determined for a subset of 15 compounds in the training set.

2. Materials and methods

2.1. Materials

Eighty-eight J&J compounds with in-vivo LogBB, data were obtained from the J&JPRD compound library (Beerse, Belgium) for evaluation. The following quality control compounds and solvents were purchased from Sigma (Bornem, Belgium): caffeine, clonidine, diazepam theophilline, verapamil dodecane and DMSO. The BLM (black lipid membrane) solution, the GIT (gastro intestinal tract) lipid solution, the system solution concentrate, a proprietary buffer for performing PAMPA, the acceptor sink buffer, a proprietary acceptor solution for performing Double Sink assays, the PAMPA 96-well sandwiches (a disposable top [with 0.45 μm PVDF filter] and bottom plate), the deep well mixing plates, the V-bottom stock plates, the high sensitivity UV plates, disposable tips, the Gut-Box™ a mechanical stirring apparatus and coated stirrers were purchased from pION Inc. (Woburn, MA, USA). The porcine polar brain lipid (PBL) was obtained from Avanti Polar Lipids Inc. (Alabaster, AL, USA). Methanol, acetonitrile and formic acid were purchased from Biosolve (Valkenswaard, The Netherlands). Caco-2 cells were obtained from the American type culture collection (ATCC). The culture medium, Dulbecco's modified eagle medium (DMEM), was supplemented with 1% non-essential amino acids (NEAA), the transport medium Hanks' balanced salt solution (HBSS) and Trypsin-EDTA were obtained from GIBCO (Carlsbad, CA, USA). MultiScreen™ Caco-2 96-well plates (MACAC02S5) and transport plates (MACAC0RS5) were from Millipore (Brussels, Belgium). Culture flasks were from BD Biosciences (Erembodegem, Belgium). Hepes was purchased from Sigma (Bornem, Belgium). For the plasma protein binding experiments, KH_2PO_4 and $Na_2HPO_4{\cdot}2H_2O$ were purchased from Sigma (Bornem, Belgium) and the Dianorm system with macro-1 Teflon cells and Diachema 10.17 dialysis membranes (MW cut-off 10000) was used in the experimental protocol.

2.2. Compound selection and chemical diversity

Compounds derived from the J&J compound database with available rat brain distribution data obtained after oral (PO) and/or subcutaneous (SC) administration were identified and selected. The in-vivo brain distribution experiments were performed as previously described (Mensch et al., 2010) and were carried out in accordance with appropriate local, national and European animal care and use regulations including EC Directive 86/609/EEC. The brain distribution experiments allowed for the determination of the LogBB values of the tested compounds. LogBB is the logarithm of the ratio of the steady-state total concentration of a compound in the brain to that in the blood/plasma. Compounds with LogBB values determined at one time point were not incorporated in the study as these data are less reliable. Thus, LogBB values were determined from the areas under the curve for brain and plasma concentrations (AUC_{brain} in h ng/g; AUC_{plasma} in h ng/ml) to eliminate the time dependence of the resulting brain/plasma ratio:

$$\mathrm{LogBB} = \log\left[\frac{AUC_{brain}}{AUC_{plasma}}\right] \quad (0)$$

Compounds with a LogBB < 0 or a LogBB ≥ 0 are classified as BBB− or BBB+ compounds, respectively.

In addition, to ensure a chemically diverse training set, a clustering analysis was performed based on the Tanimoto distance metric between fingerprints of two molecules. The fingerprint generation algorithm examines a molecular structure and finds all relevant substructures where a substructure represents atoms and bonds and their nearest neighbors up to seven bonds away. Substruc-

Table 1
Characteristics of the different PAMPA models. Lipid charge is expressed as negative: zwitterionic lipid ratio (exclusive of cholesterol and triglycerides).

	PAMPA-BLM	PAMPA-BBB	PAMPA-DS	PAMPA-BBB-UWL
Sink	No	No	Yes	No
Membrane	2% DOPC	2% PPBL	20% soy lecithin	2% PPBL
Lipid charge	Neutral	1:2.0	1:2.9	1:2.0
Incubation	18 h	18 h	4 h	1 h
Stirring	No	No	No	Yes (60 μm)

tures are then represented by bits in the fingerprint, resulting in one fingerprint per molecule.

The result of the Tanimoto distance calculation between two fingerprints is a value between 0 and 1 with 0 indicating no similarity and 1 indicating 100% similarity. As a guideline, a Tanimoto distance of 0.7 or above is representative of two molecules having structural similarity. This cut-off was then utilized to cluster the selected compounds, which can then be used to assess the chemical diversity.

2.3. Determination of thermodynamic solubility

In order to control for precipitation of compounds in the PAMPA experiments, the thermodynamic solubility of the selected compounds was determined in the universal pION system solution concentrate, adjusted with 0.5 M KOH to a pH of 7.4. The thermodynamic solubility protocol was described previously in detail (Mensch et al., 2010). In short, an aliquot of the pION buffer pH 7.4 was saturated with an excess of the compound, equilibrated at ambient temperature overnight and filtered through a 0.45 μM filter tip (disc) (Millipore (Brussels, Belgium)). Samples were analyzed and the concentration calculated (Mensch et al., 2006). All PAMPA experiments were conducted at 90% of the maximum solubility of the J&J compounds to reduce the potential for precipitation during the permeability experiments.

2.4. PAMPA-BLM procedure

The PAMPA-BLM (Table 1) was performed in a 96-well sandwich plate format similar to that described in the literature (Mensch et al., 2010, 2006; Instruction Manual for PAMPA Evolution Permeability Analyzer, version 2.2.0, 2004). A Tecan Genesis robotic system with an eight-probe liquid handling arm was used to perform all solution transfers. The quality control compounds were dissolved in DMSO (10 mM) and were subsequently diluted 200× in the pION buffer (pH 7.4) to a final reference concentration of 50 μM. The quality controls were used in each PAMPA model. The test compounds were dissolved in DMSO to a concentration such that after dilution (200-fold), a final reference concentration of 90% of their thermodynamic solubility in the pION buffer at pH 7.4 was provided.

The UV spectrum (250–500 nm) of a reference solution was measured using a 96-well plate reader (Molecular Devices, model 190 Spectramax, Sunnyvale, CA, USA). The pION bottom plate was then filled with the reference solutions to prepare the 'donor' wells. Subsequently, the membranes of a 96-well polyvinylidene fluoride (PVDF) filter (acceptor) plate were coated with 4 μl of the BLM solution, a 2% (w/v) dodecane solution of dioleoylphosphatidylcholine. All acceptor wells were filled with 200 μl of pION buffer pH 7.4 and the acceptor plate was placed on top of the donor plate to create a "sandwich" in which two compartments were separated by the coated filter. The created "sandwich" was then incubated at 22 °C for approximately 18 h. After this incubation time, the PAMPA sandwich was disassembled and the donor and acceptor solutions were transferred to disposable high sensitivity UV plates (pION Inc., Woburn, MA, USA). The amount of drugs in the donor and acceptor wells was determined by UV spectroscopy wherein absorbance between 250 and 500 nm was measured. In cases where UV spectra could not be obtained due to poor sensitivity, samples were transferred to an Acquity UPLC/MS/MS system (Waters Milford, MA, USA) and were analyzed using a generic UPLC/MS/MS method (Mensch et al., 2006). The PAMPA Evolution version 2.2 was used to calculate the effective permeability taking into account iso-pH conditions and membrane retention of the drug molecule:

$$P_{eff} = -\frac{2.303V_d}{A\left(t-\tau_{lag}\right)}\left(\frac{1}{1+r_v}\right)\cdot\log_{10}\left[-1+\left(\frac{1+r_v^{-1}}{1-R}\right)\cdot\frac{Ca(t)}{Cd(0)}\right] \quad (1)$$

with the aqueous compartment volume ratio, $r_v = \frac{V_d}{V_a}$ (in this case $r_v = 1$), V_d = volume of donor well, V_a = volume in acceptor well, A = filter area, t = permeation time, τ_{lag} = time needed to saturate the membrane, R = mole fraction of solute lost to the membrane, Cd and Ca = concentration in donor and acceptor well. All compounds were tested in triplicate at pH 7.4 and the average of the three experiments is reported.

In a previous study (Mensch et al., 2010), the PAMPA-BLM assay, was found to correctly classify ($P_{eff} < 2 \times 10^{-6}$ cm/s = BBB− and $P_{eff} \geq 2 \times 10^{-6}$ cm/s = BBB+) a set of compounds with the exception of three substances which were categorized as false positives. The obtained efflux ratios of the three false positive outliers showed moderate efflux effects (efflux ratio > 2) which suggest that misclassification could be attributed to the effect of P-gp related efflux.

2.5. PAMPA-BBB procedure

The PAMPA-BBB model (Table 1) applied in this study was based on the BBB model described in literature (Di et al., 2003; Mensch et al., 2010). The experimental procedure, conditions and P_{eff} calculation of the PAMPA-BBB model were identical to those of the above-mentioned PAMPA-BLM model with the exception of the artificial lipid membrane used. The lipid membrane of the PAMPA-BBB model was prepared by dissolving 20 mg of porcine polar brain lipid (PBL) in 1 ml dodecane. The filter membranes of the PAMPA-BBB model were coated with 4 μl of the porcine PBL solution. With this setup of identical experimental conditions, the ability of both artificial lipid formulations (BLM versus PBL) to provide the required BBB classification could be evaluated.

Previously (Mensch et al., 2010), the PAMPA-BBB model classified 13 compounds correctly as BBB+ or BBB− compounds from a set of 14 compounds ($P_{eff} < 4 \times 10^{-6}$ cm/s = BBB− and $P_{eff} \geq 4 \times 10^{-6}$ cm/s = BBB+). Only one compound appeared to manifest a false positive outcome and this compound was shown to be a substrate for moderate efflux (efflux ratio > 2).

2.6. PAMPA-DS procedure

The PAMPA-Double Sink method (Table 1) has become the working standard in pharmaceutical industry for the prediction of intestinal absorption (Avdeef et al., 2007). In the Double Sink (DS) model (Avdeef, 2003a,b; Mensch et al., 2010) applied in this study,

surfactant is added to the acceptor buffer (pH 7.4) to create sink conditions by solubilizing lipophilic molecules that permeated the artificial lipid membrane. For this reason, the permeability equation applied for the PAMPA-BLM and PAMPA-BBB (Eq. (1)) describing the non-sink process is inappropriate for the PAMPA-DS model. In the PAMPA-DS mode, it can be assumed that the reverse transport is effectively zero. Consequently, the permeability equation (Eq. (1)) can be simplified to (Avdeef, 2003a):

$$P_{eff} = -\frac{2.303V_d}{A\left(t-\tau_{lag}\right)} \cdot \log_{10}\left[\left(\frac{1}{1-R}\right) \cdot \frac{Cd(t)}{Cd(0)}\right] \quad (2)$$

The experimental procedure of the PAMPA-DS model is similar to that of the above-mentioned PAMPA models but some experimental conditions are modified. Besides the use of sink conditions in the acceptor compartment, a different artificial lipid solution is applied on the filter membrane (4 μl). This GIT lipid solution (pION Inc., Woburn, MA, USA) consists of 20% soy lecithin dissolved in dodecane (Mensch et al., 2010). In addition, the incubation time was decreased from 18 h (for PAMPA-BLM and PAMPA-BBB) to 4 h for PAMPA-DS at 22 °C. In addition to these changes, another consequence of the addition of the surfactant to the acceptor compartment was the increase in the background signal in the mass spectrometer such that no daughter ions could be detected. The use of the surfactant, thus, restricted the analytical possibility to only UV spectrophotometry.

2.7. PAMPA-BBB-UWL procedure

The in-vitro permeability cell-culture or PAMPA models can underestimate the true membrane permeability because of the unstirred water layer (UWL) (Avdeef, 2003a). The in-vivo UWL is usually significantly smaller than the UWL associated with in-vitro models (Pardridge, 1991). The PAMPA-BBB-UWL model (Table 1) applied in this study was already described previously (Mensch et al., 2010). In short, all donor wells contained a coated magnetic stirrer which was individually tumbled by using the GutBox(R) (pION Inc., Woburn, MA, USA), a mechanical stirring apparatus to decrease the UWL of the donor compartment to 60 μm. The PAMPA-BBB-UWL model used a similar experimental procedure and P_{eff} calculation (Eq. (1)) to those discussed in the PAMPA-BLM and PAMPA-BBB models. In fact, the PAMPA-BBB-UWL model was developed based on the PAMPA-BBB method. In both models, exactly the same artificial lipid solution was prepared by dissolving 20 mg of porcine polar brain lipid (PBL) in1 ml dodecane. The filter membranes of the PAMPA-BBB-UWL model were also coated with 4 μl of the porcine PBL solution. On the other hand, the differences in experimental conditions compared to the PAMPA-BBB method included the decrease in incubation time to 1 h by using the GutBox(R) and the resulting UWL of 60 μm.

It can be assumed that the overall resistance to passive transport (inverse of permeability) is the sum of the resistances of the UWL, at both sides of the membrane, and the membrane:

$$\frac{1}{P_{eff}} = \frac{1}{P_u^D} + \frac{1}{P_m} + \frac{1}{P_u^A} \quad (3)$$

where P_m is the permeability of the membrane, P_u^D and P_u^A are the UWL permeability coefficients on the donor and acceptor sides, respectively.

The UWL is characterized by the water diffusivity (D_{aq}) of the drug divided by the thickness of the layer (h):

$$P_u = \frac{D_{aq}}{h} \quad (4)$$

Reducing the UWL in the donor compartment affects the overall resistance and hence the effective permeability. Because of the vigorous agitation, UWL's smaller than 60 μm resulted in increased variability of P_{eff} among all individual wells (Brewster et al., 2007).

2.8. Caco-2 bidirectional assay

Caco-2 cells were obtained from the American type culture collection (ATCC), and were used between a passage number of 40 and 60. The cells were maintained in 175 cm^2-plastic culture flasks (BD Biosciences, Erembodegem, Belgium) and were subcultured before reaching confluence. Caco-2 cells were detached with 0.05% trypsin-EDTA (Gibco) for 15 min at 37 °C and seeded in new flasks. The culture medium, Dulbecco's modified eagle medium (DMEM), was supplemented with 1% non-essential amino acids (NEAA). The cells were seeded in 96-well MultiScreen Caco-2 (Millipore, Brussels) at 9000 cells/well and the plates were cultured for 21 days. They were fed basolaterally and apically with 250 μl and 75 μl, respectively, of fresh medium every other day, and were incubated at 37 °C and 5% CO_2. After 7 days, the cells form a full monolayer and, after 21 days, they were fully differentiated and ready for transport experiments.

Prior to the transport experiments, the medium from the basolateral and apical side was replaced with 250 and 75 μl of pre-warmed HBSS (25 mM Hepes buffer, pH 7.4), respectively. The plates were allowed to equilibrate for 30 min at 37 °C and 5% CO_2 on a shaker (KS125 basic) at 80 rpm. Subsequently, the integrity of the cell monolayers was determined by measurement of the transepithelial electrical resistance (TEER). The resistance of the cell monolayers grown on 96-well MultiScreen Caco-2 plates was measured using an Evom resistance voltohm meter (World Precision Instruments, Berlin, Germany). All wells with TEER values less than 200 Ω cm^2 were discarded.

For the apical to basolateral (A–B) transport, the buffer was removed from the cells and replaced with 75 μl of the test compound solution (20 μM) on the apical side while the basolateral compartment was replaced with 250 μl of the pre-warmed HBSS buffer. For the basolateral to apical (B–A) transport, the buffer was removed from the cells and replaced with 250 μl of the test compound solution (20 μM) on the basolateral side while the apical compartment was replaced with 75 μl of the pre-warmed HBSS buffer. The monolayers were incubated for 120 min at 37 °C, 5% CO_2, and shaken at 80 rpm. The amount of drug accumulated in the basal compartment was determined at different time-points: 30, 60, 90 and 120 min. At each time point, the entire solution volume from the basolateral side was sampled and replaced with 250 μl of fresh and pre-warmed HBSS buffer for the A–B transport experiments. Likewise for the B–A experiments, the entire volume from the apical side was sampled and replaced with 75 μl of fresh and pre-warmed HBSS buffer. All samples were diluted with acetonitrile (1:1 v/v) prior to analysis with the Acquity UPLC/MS/MS system (Mensch et al., 2006) (Waters Milford, MA, USA). A US Food and Drug Administration (FDA) standard, carbamazepine, was included in all plates as a quality control to monitor the consistency of the permeability test. The observed variability of both the A–B and the B–A permeability for carbamazepine was less than 5%.

At the end of the transport experiments, the cell monolayers were rinsed with HBSS buffer and incubated with 75 μl of a sodium fluorescein solution (1 mg/ml in HBSS) in the apical compartment and 250 μl HBSS buffer at the basolateral side for an additional time of 60 min at 37 °C, 5% CO_2 and shaken at 80 rpm. To assess the paracellular transport, 100 μl from the basolateral side was sampled to determine the diffusion of sodium fluorescein into the basal compartment. The diffusion of sodium fluorescein was determined by measuring the fluorescence intensity (excitation 490 nm, emission 514 nm) using a Tecan Genios (Tecan Benelux, Mechelen) fluorimeter.

Final concentrations in the apical and basolateral compartment were quantified by interpolation of the calibration data. Apparent permeability (P_{app}) values were calculated algebraically:

$$P_{app} = \left[\frac{\text{amount measured in receiver}\,(\mu g)}{\text{area of cells}\,(0.11\ \text{cm}^2) \times \text{duration}\,(7200\ \text{s}) \times \text{starting concentration donor}\,(\mu g/\text{cm}^3)} \right] \quad (5)$$

Additionally, the efflux ratio could be determined whereby the B–A apparent permeability was divided by the A–B apparent permeability. Compounds with an efflux ratio higher than 2 were categorized as substrates for efflux mechanisms.

2.9. Plasma protein binding experiments

Plasma protein binding of drugs has been shown to have significant effects on different aspects of (clinical) pharmacokinetics and pharmacodynamics (Jeffrey and Summerfield, 2007; Hammarlund-Udenaes et al., 2008; Maurer et al., 2005; Summerfield et al., 2006). Although it is assumed that plasma protein bound drug is not available for transport through the BBB, studies have shown that many plasma protein bound compounds are available for penetration through the BBB (Pardridge, 1995).

In the experimental PPB protocol, blank plasma of rat was fortified with the compound at a concentration of 5 μM. The samples were subjected to equilibrium dialysis against a 0.067 M phosphate buffer (pH 7.17) at 37 °C for 4 h in a Dianorm system with macro-1 Teflon cells and Diachema 10.17 dialysis membranes (MW cut-off 10000) allowing the unbound drug to diffuse into the phosphate buffer. Rat plasma was selected because all in-vivo LogBB experiments were conducted in rats. The dialysis experiments were performed in triplicate. After dialysis, the contents of the two compartments of the dialysis cells were collected separately. The volume of the contents of the buffer compartments was determined by weighing; subsequently, it was mixed with 0.1 ml aliquots of 10% bovine serum albumin (BSA) solution after dialysis, in order to avoid the possible adsorption of the compounds from the buffer solutions to the glass tubes or to the disposable tips used for sampling. Individual samples were analyzed by an appropriate bioanalytical method.

To investigate the plasma protein binding, the fraction unbound (f_u) is calculated as follows:

$$f_u = \frac{C_u}{C} \quad (6)$$

whereby C_u is the concentration unbound and C the total concentration of the compound. C_u and C are determined by measurement of the concentration of the drug in the buffer compartment of the Dianorm cell and the plasma compartment. To compensate for differences in PPB, LogBB_u, u compares the total brain drug concentrations with plasma concentrations of unbound drug:

$$\text{LogBB}_u = \frac{AUC_{brain}}{f_{u,plasma} \times AUC_{plasma}} \quad (7)$$

2.10. Calculation physicochemical parameters

For compounds with measured PAMPA values and LogBB values, physicochemical properties were calculated using the Pipeline Pilot software (Accelrys) and the MOE package (Chemical Computing Group). The following molecular properties were determined as a basic set with Pipeline Pilot: molecular weight, number of hydrogen acceptors and donors, number of rotatable bonds, number of rings, number of atoms, number of aromatic rings, molecular volume, molecular polar surface area, clog P, different clog D values, calculated molecular refractivity, max pKb, min pKa, Bpol (sum of the absolute value of the difference between atomic polarizabilities of all bonded atoms in the molecule), molecular mass density, van der Waals area and topological polar surface area.

Other structural properties of the compounds were calculated using MOE. These properties describe two and three dimensional properties of the molecule such as volume, shape or charge density. Properties that were highly cross-correlated were removed. All together, around 200 descriptors were generated by MOE.

2.11. Modeling linear relationships between descriptors and LogBB's

A useful statistical method applied in the prediction of BBB permeation is multiple linear regression (MLR) (Abraham et al., 2006b; Rose et al., 2002; Konovalov et al., 2007; Clark, 1999; Wichmann et al., 2007). This classical approach to regression problems was implemented, assuming that the predictor variables, normally called X (descriptor space), are orthogonal (mathematically independent). A limitation of MLR is the sensitivity to correlated descriptors. MLR is satisfactorily applied if it is assumed that the descriptors are exact and completely relevant for the modelling of the biological response under study.

Besides MLR, other statistical methods such as principal component regression (PCR) and especially partial least squares (PLS) analysis are increasingly used and have been applied in the prediction of BBB penetration. These multivariate projection methods are particularly suitable when the number of variables equals or exceeds the number of compounds. PLS exists in many different forms and approaches. The two-block predictive PLS version (McIntosh et al., 1996; Wold et al., 2001) is the most often used model in science and technology. This method is applied for relating two data matrices, X and Y, by a linear multivariate model. PLS is able to analyze data with many, noisy, co-linear and even incomplete variables in both X and Y domains. PLS has the desirable property that the precision of the model parameters improves with the increasing number of relevant variables and observations. In fact, PLS has been successfully applied in the prediction of BBB permeation (Urbano-Cuadrado et al., 2007; Sun, 2004).

In this work, two statistical methodologies were applied using the PAMPA data and the calculated physicochemical and/or structural compound parameters to predict LogBB.

First, collected data (PAMPA, physicochemical and structural descriptors) were analyzed by the SimcaP + 12 software (Umetrics) to find relations between the independent variables and LogBB. Initially, a principal component analysis was performed on the X-block (predictor variables) to see if the dataset contained outliers. Subsequently, a PLS was performed.

Secondly, MLR with backward stepwise selection was performed to model LogBB (independent variable) with the PAMPA values of flux, P_{eff} and retention, and the calculated physicochemical parameters (Statgraphics Centurion XVI). This technique starts with a model including all parameters and the procedure removes parameters, one at a time, if they do not contribute in a statistically significant way ($p > 0.05$) to optimize the model. Removed variables can be added to the model at later steps if they become statistically significant ($p < 0.05$). This approach can lead to a more optimized MLR model for LogBB.

Table 2
Obtained PAMPA data [P_{eff} (10^{-6} cm/s), Flux(μg/s cm), Ret (%)] for all four PAMPA-models ($N = 3$). –: no data available. equi: equilibrated concentration of the compound in donor and acceptor compartment and represents high permeable compounds.

Compounds	LogBB	PAMPA-BLM			PAMPA-DS			PAMPA-BBB			PAMPA-BBB-UWL		
		P_{eff}	Flux	Ret	P_{eff}	Flux	Ret	P_{eff}	Flux	Ret	P_{eff}	Flux	Ret
J&J-1	1.32	13.61	111.18	67	61.90	505.78	40	29.45	240.66	68	18.61	152.06	62
J&J-2	−0.24	1.15	9.97	–	84.93	734.86	43	–	–	–	15.18	131.36	97
J&J-3	−0.89	2.26	3.39	66	9.52	14.27	35	4.95	7.42	56	0.00	0.00	0
J&J-4	−0.80	4.66	49.65	15	56.55	602.94	24	10.68	113.82	29	0.71	7.54	90
J&J-5	−0.64	5.54	98.18	62	38.90	689.24	51	5.93	105.05	73	21.93	388.58	98
J&J-6	0.08	22.21	180.69	43	46.92	381.68	19	23.28	189.37	39	114.35	930.28	42
J&J-7	−0.10	0.04	0.44	46	42.30	454.60	46	12.07	129.70	61	26.85	288.61	59
J&J-8	1.04	15.26	217.26	54	65.52	932.72	37	6.17	87.89	59	2.45	34.90	11
J&J-9	1.99	–	–	–	64.62	209.29	22	–	–	–	58.95	190.95	77
J&J-10	−0.46	3.27	5.26	72	65.40	105.21	0	0.08	0.12	96	–	–	–
J&J-11	−0.35	14.31	236.99	68	2.28	37.72	61	0.00	0.00	78	28.49	472.07	93
J&J-12	−0.80	0.00	0.00	4	6.00	49.87	10	1.55	12.88	6	0.21	1.75	17
J&J-13	−1.10	0.00	0.00	56	41.36	41.48	0	0.00	0.00	37	0.00	0.00	27
J&J-14	−0.81	–	–	–	17.60	6.92	0	–	–	–	–	–	–
J&J-15	−1.40	0.02	0.24	1	1.04	10.67	16	0.08	0.81	3	0.00	0.00	20
J&J-16	−0.42	0.02	0.17	31	46.76	342.07	12	1.53	11.22	26	0.00	0.00	36
J&J-17	−0.43	0.06	0.61	31	40.00	375.46	25	0.35	3.24	28	0.00	0.00	32
J&J-18	1.51	–	–	–	–	–	–	–	–	–	–	–	–
J&J-19	−0.62	0.76	7.43	11	66.84	655.91	17	5.99	58.81	21	0.31	3.06	46
J&J-20	−0.96	14.57	28.15	47	61.98	119.81	1	13.85	26.78	38	–	–	–
J&J-21	−2.00	5.26	17.70	53	46.05	155.07	10	18.10	60.94	45	91.52	308.17	61
J&J-22	0.68	17.43	136.17	28	65.20	509.30	15	1.30	10.12	29	6.17	48.21	5
J&J-23	2.35	35.15	394.98	27	74.99	842.70	15	15.34	172.39	38	77.86	874.93	81
J&J-24	−0.77	0.00	0.00	27	14.40	118.87	58	7.64	63.06	40	64.49	532.45	35
J&J-25	0.23	2.25	33.51	–	28.93	430.29	41	–	–	–	45.96	683.65	100
J&J-26	−1.00	3.54	58.97	31	51.34	855.67	44	6.25	104.11	53	90.51	1508.55	96
J&J-27	1.34	–	–	–	–	–	–	–	–	–	–	–	–
J&J-28	−0.55	0.00	0.00	–	83.34	149.12	1	4.90	8.76	47	0.00	0.00	31
J&J-29	0.87	17.96	148.96	73	46.56	386.28	41	4.48	37.13	83	35.22	292.17	46
J&J-30	1.37	17.67	153.63	65	30.72	267.19	30	8.61	74.85	89	358.52	3117.86	30
J&J-31	0.54	20.74	117.45	82	31.15	176.41	58	18.36	103.94	80	81.74	462.85	3
J&J-32	1.06	–	–	–	34.75	41.08	59	–	–	–	–	–	–
J&J-33	0.64	–	–	–	–	–	–	–	–	–	263.15	1491.42	43
J&J-34	0.28	3.89	41.18	15	91.07	964.28	3	9.32	98.67	20	1.99	21.11	79
J&J-35	−1.00	12.15	115.25	33	29.63	281.02	46	12.82	121.63	51	93.73	889.05	52
J&J-36	1.32	9.90	3.20	88	79.82	25.80	6	17.78	5.75	93	–	–	–
J&J-37	1.21	25.09	189.92	19	89.12	674.63	29	9.77	73.97	43	35.95	272.14	9
J&J-38	−0.15	–	–	–	–	–	–	–	–	–	0.00	0.00	96
J&J-39	−0.46	–	–	–	–	–	–	–	–	–	73.52	493.21	49
J&J-40	−0.05	19.63	295.06	63	158.99	2389.63	16	11.03	165.81	73	equi	–	–
J&J-41	−0.40	16.57	186.13	47	46.12	518.07	10	23.07	259.09	38	109.97	1235.21	11
J&J-42	−0.52	9.92	125.72	20	36.50	462.57	37	13.38	169.58	26	23.39	296.39	20
J&J-43	2.02	16.70	228.59	16	45.52	623.05	32	13.36	182.82	29	8.89	121.73	89
J&J-44	−1.40	0.00	0.00	2	2.61	11.08	8	0.03	0.13	5	2.38	10.08	2
J&J-45	0.48	14.09	155.58	50	60.27	665.36	37	33.34	368.09	52	197.99	2185.57	86
J&J-46	−1.00	0.00	0.00	8	19.34	191.42	41	3.80	37.62	15	1.02	10.09	0
J&J-47	0.70	13.62	128.30	53	53.18	501.13	48	3.84	36.18	94	22.40	211.09	100
J&J-48	1.58	13.36	49.70	64	40.80	151.84	59	6.94	25.82	89	39.77	147.99	18
J&J-49	−0.54	–	–	–	36.07	88.55	81	0.00	0.00	–	0.00	0.00	16
J&J-50	−0.52	22.22	240.30	32	58.78	635.60	33	16.67	180.22	27	83.73	905.40	0
J&J-51	1.20	21.91	168.85	52	63.73	491.21	35	9.52	73.35	55	20.47	157.77	5
J&J-52	−0.74	11.03	100.54	12	23.55	214.59	22	10.72	97.65	12	8.73	79.56	0
J&J-53	−0.22	3.56	26.81	15	30.90	232.98	14	1.72	12.96	17	7.47	56.30	12
J&J-54	0.20	–	–	–	42.60	563.95	63	–	–	–	15.35	203.15	35
J&J-55	−1.10	3.57	34.31	30	50.77	488.46	27	1.44	13.85	4	0.00	0.00	10
J&J-56	0.97	9.91	35.37	68	47.08	168.09	66	0.32	1.14	99	93.36	333.34	24
J&J-57	0.11	14.01	38.53	47	46.25	127.19	32	5.22	14.37	41	67.77	186.36	0
J&J-58	−1.40	0.48	5.72	19	33.16	392.63	31	4.34	51.41	13	6.22	73.58	0
J&J-59	−0.15	12.37	134.35	25	58.49	635.36	28	3.13	34.04	47	9.51	103.34	25
J&J-60	−0.96	1.06	1.73	68	–	0.00	–	3.66	5.99	41	107.96	176.52	0
J&J-61	−1.05	3.27	3.87	88	62.91	74.32	34	12.30	14.54	31	126.02	148.89	53
J&J-62	0.68	17.38	190.70	56	86.22	946.17	31	5.89	64.68	78	20.89	229.22	30
J&J-63	0.04	0.00	0.00	23	29.43	346.28	32	6.59	77.56	32	42.73	502.69	8
J&J-64	−1.00	17.82	184.23	25	51.37	531.13	27	17.54	181.31	23	38.70	400.05	19
J&J-65	−1.00	3.22	9.85	27	57.28	175.08	26	8.45	25.81	23	11.09	33.90	27
J&J-66	0.57	16.61	168.01	29	61.48	621.71	29	15.82	160.00	53	114.70	1159.96	83
J&J-67	0.87	13.81	206.53	62	64.14	959.08	35	4.26	63.69	85	18.58	277.83	99
J&J-68	−1.22	2.40	24.50	7	18.24	186.30	13	2.75	28.07	6	1.32	13.50	0
J&J-69	0.30	8.74	159.95	98	64.27	1176.02	11	–	–	–	105.89	1937.60	98
J&J-70	−0.30	3.03	45.14	23	55.37	825.93	35	12.73	189.88	21	60.83	907.29	85

Table 2 (*Continued*)

Compounds	LogBB	PAMPA-BLM			PAMPA-DS			PAMPA-BBB			PAMPA-BBB-UWL		
		P_{eff}	Flux	Ret	P_{eff}	Flux	Ret	P_{eff}	Flux	Ret	P_{eff}	Flux	Ret
J&J-71	0.68	26.83	302.85	47	73.66	831.59	45	0.42	4.75	8	7.73	87.30	27
J&J-72	0.00	21.20	120.72	64	60.80	346.19	35	8.53	48.56	57	22.50	128.11	5
J&J-73	−0.10	4.47	2.15	77	–	–	–	–	–	–	equi	–	–
J&J-74	−1.30	8.01	80.34	33	36.65	367.70	33	10.82	108.57	22	11.55	115.82	5
J&J-75	1.08	17.24	132.86	23	46.84	361.01	39	17.13	132.04	60	35.61	274.47	44
J&J-76	−0.30	2.72	31.42	29	51.96	601.23	40	4.36	50.40	7	20.53	237.61	12
J&J-77	−1.22	18.64	165.02	36	58.09	514.16	31	18.97	167.91	31	71.35	631.47	27
J&J-78	0.11	0.04	0.42	10	1.76	17.71	71	2.83	28.45	72	19.78	198.52	41
J&J-79	−0.49	0.00	0.00	38	47.89	229.14	11	10.03	48.02	61	24.91	119.21	65
J&J-80	−0.70	16.86	172.98	19	62.44	640.75	36	13.96	143.26	31	3.60	36.98	62
J&J-81	−0.15	16.37	153.86	47	89.77	843.53	0	25.67	241.20	45	37.90	356.13	33
J&J-82	0.28	13.28	97.98	39	78.40	578.31	15	5.72	42.21	78	93.82	692.08	99
J&J-83	−0.49	0.03	0.29	29	56.05	517.78	43	12.41	114.64	46	27.91	257.79	52
J&J-84	−0.41	5.55	46.13	50	61.26	508.82	44	18.22	151.32	30	46.09	382.78	61
J&J-85	−0.44	2.31	19.76	18	56.47	483.17	23	12.72	108.83	16	30.35	259.66	23
J&J-86	−0.05	3.86	31.96	29	43.78	362.64	36	14.86	123.09	18	30.12	249.51	39
J&J-87	0.60	4.66	35.72	11	60.79	465.65	27	9.89	75.75	25	12.31	94.29	47
J&J-88	−0.60	0.01	0.05	6	47.96	477.05	19	3.75	37.34	16	7.82	77.79	14

3. Results and discussion

3.1. Compound selection and chemical diversity

Compounds were selected based on available LogBB values obtained from the areas under the curve for brain and plasma concentrations after PO and/or SC administration. These selection criteria led to a set of 117 compounds with available in-vivo brain distribution data. These compounds were evaluated for their chemical diversity by performing a clustering analysis using the Tanimoto distance with a 0.7 cut-off. The compounds could be divided in 58 chemically different clusters demonstrating the chemical diversity of the set.

3.2. Evaluation with the PAMPA models and in-vivo LogBB data

Prior to the PAMPA experiments, the thermodynamic solubility in pION buffer at pH 7.4 was determined. The solubility of 29 compounds was below the detection limit of the analytical method reducing the compound set to 88 compounds. All PAMPA experiments were conducted at 90% of the maximum solubility of the compounds to reduce the potential of precipitation during the permeability experiments. In this way reliable PAMPA data were obtained as together with the results of the quality control compounds which show consistent P_{eff} values inherent to each PAMPA model.

The results (P_{eff}, flux and percent retention of the drug) obtained with the four PAMPA models and the LogBB values are presented in Table 2. The flux (μg/s cm) was calculated by multiplying the P_{eff} with the $Cd(0)$ and the % retention was determined as follows: $100 \times [Cd(t) + Ca(t)]/Cd(0)$. The LogBB of the compounds was determined based on multiple time-points after oral or subcutaneous administration to eliminate the time dependence of the resulting brain/plasma ratio. In those cases where compounds were administered both PO and SC, no differences in LogBB values were evident (Mensch et al., 2010).

3.3. Calculation physicochemical parameters

From all 88 compounds, the physicochemical properties were calculated using the Pipeline Pilot software package (Accelrys) (Tables 3 and 4). These parameters were used as input parameters to model LogBB.

More complex structural properties of the compounds were calculated using MOE. These properties describe 2D and 3D properties of the molecule such as volume, shape or charge density. Properties that were highly correlated were removed. All told around 200 descriptors were generated by the MOE software (data not shown).

3.4. PLS modeling of LogBB

The question to be answered in this experimental phase was whether prediction of brain penetration (LogBB) could benefit from inclusion of experimental PAMPA results, and if so, which PAMPA model contributes most significantly. Initially, a principal component analysis was performed on all variables to identify outliers in the dataset. The PCA showed that the compounds are regularly distributed within the PCA-space resulting in a good representation of the entire dataset (Fig. 1).

Subsequently, a PLS analysis was applied to generate different and optimized models to predict LogBB. A variety of models were constructed, to investigate the effect of different properties (Table 5): with models 1–4 including the basic physicochemical properties and PAMPA results per assay (P_{eff}, flux and % retention) separately, model 5 representing the compounds described by the basic physicochemical properties without PAMPA results, models 6–9 associated with compounds described by the basic physicochemical properties and MOE-descriptors together with results from PAMPA assays and model 10 giving compounds described by the basic physicochemical and MOE-descriptors without PAMPA results. The predictive power of the models was evaluated using R^2 and Q^2 values. R^2 is an estimate of the goodness-of-fit and Q^2 is an estimate of the goodness-of-prediction. The results (Table 5) indicate that the PAMPA parameters improve the predictive power of the PLS models to predict LogBB but the increase in R^2 is small. Model 5, containing only the physicochemical parameters as independent variables (X-variables), explains 52.0% of the variability in LogBB, while including the parameters from the four PAMPA-models separately, R^2 increases to 59.1%, 57.6%, 59.7% and 52.3% for PAMPA-BLM, PAMPA-DS, PAMPA-BBB and PAMPA-BBB-UWL, respectively. Modeling LogBB from a set of physicochemical and PAMPA properties explains ±60% of the variability. Similar results were obtained when including the MOE (2D and 3D) structural variables (Table 5); here ±77% of the variability can be explained whereby inclusion of the PAMPA-BLM parameters provides a slight improvement of the model performance.

3.5. MLR with backward stepwise selection to model LogBB

Another approach applied in this study to model LogBB is the multiple linear regression analysis with backward stepwise selec-

Table 3
Calculated physicochemical properties of the 88 J&J compounds (part 1).

Compounds	Max pKb	MW	Number of H-bond acceptors	Number of H-bond donors	Number of atoms	Number of rotatable bonds	Number of aromatic rings	Molecular volume ($Å^3$/mol)	Molecular polar surface area ($Å^2$)	Calculated molecular refractivity ($Å^3$/mol)	Bpol ($Å^3$)
J&J-1	7.14	326.8	4	1	23	1	2	218.1	30.9	9.4	27.1
J&J-2	7.52	686.7	4	0	49	8	3	429.4	47.1	17.6	60.8
J&J-3	9.31	555.5	4	1	37	8	5	356.4	45.6	15.6	40.4
J&J-4	7.86	426.5	5	1	31	4	2	277.5	82.2	11.4	38.9
J&J-5	7.4	708.8	6	0	49	8	3	437.3	101.1	17.5	62.2
J&J-6	2.6	325.4	4	0	24	3	2	219.5	48.4	9.3	31.3
J&J-7	9.75	393.5	4	1	29	9	3	260.3	49.8	11.2	32.3
J&J-8	8.32	453.4	4	1	29	3	1	286.4	47.9	11.9	35.5
J&J-9	8.45	359.9	5	0	25	5	2	257.6	35.5	10.4	37.4
J&J-10	7.34	446.9	7	1	31	8	3	285.7	68.7	11.7	38.9
J&J-11	7.4	662.7	4	0	47	8	3	408.2	60.2	16.4	58.3
J&J-12	8.12	332.4	5	1	24	3	1	220.5	66.9	9.0	37.0
J&J-13	7.68	371.4	3	1	28	8	3	249.4	53.7	11.2	27.8
J&J-14	7.68	371.4	3	1	28	8	3	249.4	53.7	11.2	27.8
J&J-15	8.59	320.3	6	2	23	6	1	203.1	92.8	8.2	32.2
J&J-16	8.59	353.4	3	1	25	7	3	232.2	81.9	10.1	27.9
J&J-17	8.59	353.4	3	1	25	7	3	232.2	81.9	10.1	27.9
J&J-18	8.79	325.4	2	0	24	2	2	225.7	12.5	9.5	31.3
J&J-19	8.3	392.5	6	2	28	7	1	275.1	80.3	10.7	44.3
J&J-20	5.06	393.4	7	1	29	10	3	261.7	74.7	11.0	36.1
J&J-21	0.93	587.1	7	2	42	7	4	374.6	115.6	15.6	44.0
J&J-22	7.26	312.4	4	1	22	1	2	212.7	59.1	9.2	30.1
J&J-23	8.05	311.4	5	1	23	5	2	228.8	44.3	9.4	34.6
J&J-24	7.42	330.2	3	2	20	4	2	206.1	99.7	8.5	20.9
J&J-25	9.34	635.7	3	0	45	7	2	407.5	43.9	16.0	57.7
J&J-26	7.4	666.7	5	0	47	8	2	426.0	56.3	16.5	62.7
J&J-27	7.78	404.4	7	1	30	4	4	260.3	75.0	11.2	33.4
J&J-28	7.86	497.0	7	3	32	8	2	317.6	159.2	12.6	41.4
J&J-29	9.49	295.4	2	1	22	2	2	200.7	21.3	8.5	23.5
J&J-30	9.57	311.4	2	1	23	2	2	213.3	21.3	9.0	27.8
J&J-31	3.9	245.1	2	1	14	1	2	148.9	67.1	6.1	10.3
J&J-32	7.98	328.4	3	3	25	6	4	218.8	52.7	10.3	25.2
J&J-33	9.54	458.5	6	0	34	8	3	299.4	68.3	12.8	40.0
J&J-34	8.54	423.5	6	1	31	10	2	281.6	69.6	12.0	43.1
J&J-35	4.68	379.4	5	1	26	6	3	226.0	109.0	9.3	29.2
J&J-36	8.39	323.2	4	1	21	4	2	203.7	41.1	8.6	22.3
J&J-37	8.74	302.8	4	1	21	4	2	202.0	41.1	8.6	25.2
J&J-38	8.06	549.7	4	0	39	10	3	389.0	64.3	15.9	56.0
J&J-39	−0.64	330.2	2	2	21	6	1	213.7	75.4	8.4	23.3
J&J-40	8.11	564.7	5	1	41	9	2	405.1	67.3	16.2	60.2
J&J-41	6.07	412.8	3	1	28	6	2	255.9	41.6	10.2	31.4
J&J-42	12.5	470.4	4	1	30	4	3	307.7	58.4	12.4	38.1
J&J-43	8.35	398.5	8	0	29	6	2	281.6	66.9	11.2	46.5
J&J-44	10.27	169.6	2	1	11	0	2	97.4	46.3	4.0	6.7
J&J-45	5.75	383.5	6	1	27	6	2	259.0	73.6	11.1	36.8
J&J-46	9.9	387.4	6	1	28	6	2	247.6	68.2	10.1	33.9
J&J-47	10.34	376.9	3	2	26	4	1	259.0	64.3	10.4	35.0
J&J-48	8.25	375.9	3	1	26	6	2	248.7	40.5	10.3	29.7
J&J-49	–	454.6	4	1	34	6	3	314.2	63.6	13.3	36.6
J&J-50	4.31	432.5	4	0	29	7	2	283.3	69.6	10.5	44.8
J&J-51	7.3	372.3	4	1	26	5	2	224.0	41.1	8.7	28.6

Table 3 (*Continued*)

Compounds	Max pKb	MW	Number of H-bond acceptors	Number of H-bond donors	Number of atoms	Number of rotatable bonds	Number of aromatic rings	Molecular volume (Å^3/mol)	Molecular polar surface area (Å^2)	Calculated molecular refractivity (Å^3/mol)	Bpol (Å^3)
J&J-52	4.24	364.5	4	0	25	5	2	256.2	69.6	10.0	42.3
J&J-53	9.53	450.5	7	1	33	11	2	296.7	75.6	12.7	45.4
J&J-54	7.52	456.6	4	2	34	6	3	314.9	76.6	13.8	42.5
J&J-55	0.03	384.8	2	1	27	5	2	249.7	49.4	10.5	25.9
J&J-56	7.79	388.9	4	2	27	4	1	263.1	57.3	10.7	37.7
J&J-57	6.79	436.5	7	1	32	10	2	279.5	75.6	12.2	43.3
J&J-58	4.33	473.6	4	0	32	8	2	307.0	80.7	11.7	49.1
J&J-59	9.54	434.5	6	1	32	10	2	288.1	66.4	12.5	43.5
J&J-60	−0.15	422.5	6	1	31	10	2	284.0	83.5	11.8	40.1
J&J-61	3.85	437.6	5	0	31	5	3	294.6	93.4	12.1	41.9
J&J-62	9.47	438.9	5	1	31	9	2	289.5	57.2	12.4	38.8
J&J-63	–	470.6	6	2	34	11	1	340.9	100.9	13.1	46.3
J&J-64	3.6	413.5	5	0	29	5	3	279.2	82.5	11.4	42.5
J&J-65	3.92	377.4	5	0	28	3	5	217.1	73.8	9.8	23.2
J&J-66	8.82	404.5	4	0	30	8	2	273.7	42.0	11.9	39.4
J&J-67	9.52	482.0	5	0	33	7	3	314.2	82.6	13.2	39.0
J&J-68	4.49	408.6	5	1	28	6	2	283.7	89.8	11.1	46.7
J&J-69	7.13	616.6	3	0	43	6	2	392.4	47.1	14.8	56.5
J&J-70	7.19	596.6	4	0	42	6	2	372.8	47.1	14.7	54.2
J&J-71	9.53	451.6	6	0	32	10	2	304.2	79.7	13.0	44.1
J&J-72	3.33	351.4	4	0	26	5	1	241.8	56.6	10.2	34.8
J&J-73	3.3	482.3	3	1	31	6	2	281.6	45.2	10.8	31.5
J&J-74	3.98	464.4	4	1	33	6	3	280.2	58.1	11.3	35.2
J&J-75	7.86	308.3	4	1	22	3	2	184.9	41.1	7.7	24.0
J&J-76	3.33	462.8	4	2	31	6	2	274.7	71.3	10.7	32.6
J&J-77	3.61	427.6	5	0	30	5	3	290.9	82.5	11.8	44.7
J&J-78	10.78	401.5	4	1	30	5	2	268.9	44.8	12.0	37.0
J&J-79	8.58	369.5	3	1	25	7	3	245.9	97.0	10.7	28.3
J&J-80	7.89	410.5	4	0	30	4	2	275.4	61.9	11.3	38.9
J&J-81	6.32	339.4	5	0	25	6	3	232.2	49.8	9.6	31.9
J&J-82	5.87	291.4	5	0	20	2	1	200.0	86.7	8.0	25.4
J&J-83	8.6	369.5	3	1	25	7	3	244.6	97.0	10.7	28.3
J&J-84	−0.64	332.2	2	2	21	7	1	218.1	75.4	8.6	25.5
J&J-85	−0.52	342.2	2	2	20	7	1	208.5	75.4	8.4	27.1
J&J-86	−0.63	331.3	2	2	23	8	1	205.5	75.4	8.1	29.4
J&J-87	9.21	306.4	3	1	23	3	3	210.9	44.8	9.3	29.3
J&J-88	8.27	397.9	6	3	27	7	1	268.6	97.1	10.5	37.8

Table 4
Calculated physicochemical properties of the 88 J&J compounds (part 2).

Compounds	clog *P*	clog *D* pH 2	clog *D* pH 5	clog *D* pH7	clog *D* pH 8	clog *D* pH 10	Density (amu/Å^3)	van der Waals area (Å^2)	Topological polar surface area (Å^2)	Min pKa
J&J-1	3.7	−0.6	2.4	3.6	3.7	3.7	0.743	320.6	30.9	–
J&J-2	4.0	−3	0.8	2.8	3.6	4	0.786	628.8	47.1	–
J&J-3	7.3	−2.9	2.8	5.2	6.2	7.2	0.760	522.5	45.6	13.05
J&J-4	1.1	−6.7	−3.5	−1.5	−0.5	0.9	0.762	393.1	82.2	12.41
J&J-5	2.5	−4.5	−0.7	1.3	2.1	2.5	0.826	631.0	72.9	–
J&J-6	3.3	−0.7	2.2	3.3	3.3	3.3	0.715	303.2	48.4	–
J&J-7	4.0	−2.9	−0.4	−0.2	−0.2	−1.3	0.720	405.5	49.8	2.33
J&J-8	4.0	−14	−7.9	−3.9	−1.9	1.2	0.806	396.1	47.9	–
J&J-9	4.1	−4.6	1.1	3.3	3.9	4.1	0.718	393.3	35.5	–
J&J-10	5.6	−2.1	3.5	5.3	5.6	5.6	0.792	425.1	68.7	–
J&J-11	3.4	−3.1	0.3	2.3	3.1	3.4	0.811	593.6	60.2	–
J&J-12	0.6	−5.2	−2.2	−0.3	0.4	0.6	0.746	326.3	66.9	14.36
J&J-13	2.7	−3.1	−0.7	−0.6	−0.9	−2.7	0.698	398.3	53.7	2.25
J&J-14	2.7	−3.1	−0.7	−0.6	−0.9	−2.7	0.698	398.3	53.7	2.25
J&J-15	-0.5	−7.3	−4.3	−2.5	−2.2	−3.4	0.780	315.2	92.8	13.06
J&J-16	2.4	−3.7	−1.3	−1.1	−1.4	−3	0.745	357.3	53.7	2.3
J&J-17	2.4	−3.7	−1.3	−1.1	−1.4	−3	0.745	357.3	53.7	2.3
J&J-18	4.6	−1.9	1.1	3	4	4.6	0.696	317.4	12.5	–
J&J-19	2.2	−5	−2	0	1	2.2	0.722	407.1	80.3	14.48
J&J-20	4.3	1.4	4.1	4.3	4.3	4.3	0.728	416.1	74.7	–
J&J-21	5.5	5.5	4.3	2.3	1.3	−0.7	0.781	516.0	115.6	3.24
J&J-22	3.0	−5.8	0.2	2.8	3	3	0.730	310.9	30.9	–
J&J-23	3.3	−7.4	−1.6	0.9	1.8	3.2	0.678	348.4	44.3	–
J&J-24	4.2	4.1	4.2	4.2	4.2	4.2	0.877	307.3	99.7	1.96
J&J-25	5.0	−3.4	−0.4	1.6	2.6	4.5	0.794	566.4	43.9	–
J&J-26	3.0	−3.6	−0.1	1.8	2.6	3	0.804	597.8	56.3	–
J&J-27	4.4	1.1	4	4.4	4.4	4.4	0.761	393.4	75.0	–
J&J-28	1.3	−5.8	−2.5	−0.5	0.4	1.3	0.836	465.9	122.5	12.25
J&J-29	3.5	−3.5	−0.5	1.5	2.5	3.5	0.718	268.7	21.3	–
J&J-30	4.0	−3.4	−0.4	1.6	2.6	3.9	0.705	290.1	21.3	–
J&J-31	3.5	1.5	3.5	3.5	3.5	3.5	0.940	207.7	38.9	–
J&J-32	4.7	−3.2	2.2	4.2	4.6	4.7	0.689	330.4	52.7	17.22
J&J-33	5.0	−1.8	1.2	3.2	4.2	5	0.738	448.1	68.3	–
J&J-34	3.0	−8.2	−2.2	1.1	2.2	2.9	0.723	446.5	69.6	–
J&J-35	4.1	4	4.1	4.1	4.1	4.1	0.855	347.6	109.0	–
J&J-36	3.9	−1.9	1.4	3.2	3.7	3.9	0.810	302.6	41.1	–
J&J-37	3.6	−3.8	−0.6	1.4	2.4	3.6	0.743	302.3	41.1	–
J&J-38	6.2	−4.9	2.5	4.7	5.6	6.2	0.714	558.2	36.0	–
J&J-39	2.7	2.7	2.7	2.7	2.7	2.7	0.839	314.0	75.4	13.31
J&J-40	5.3	−1.7	1.7	3.6	4.6	5.3	0.705	594.9	67.3	13.84
J&J-41	3.7	−0.1	2.8	3.6	3.7	3.7	0.831	375.0	41.6	13.55
J&J-42	6.8	6.3	6.3	4.5	3.5	1.5	0.793	434.2	58.4	4.66
J&J-43	3.1	−6.6	−0.8	1.5	2.5	3.1	0.715	428.3	66.9	–
J&J-44	2.5	2.5	2.5	2.5	2.5	2.5	0.927	142.2	46.3	–
J&J-45	3.0	−3.1	−0.1	1.8	2.6	3	0.734	385.7	48.3	14.41
J&J-46	1.7	−6.1	−3.5	−3.3	−3.3	−3.8	0.777	362.2	68.2	2.47
J&J-47	3.5	−5.3	−2.3	−0.3	0.7	2.7	0.736	357.0	64.4	15.02
J&J-48	3.8	−3	0	2	3	3.8	0.757	365.8	40.5	13.86
J&J-49	8.3	8.3	7.4	5.5	4.5	2.5	0.704	427.0	63.6	4.17
J&J-50	3.0	2.9	3	3	3	3	0.817	408.3	61.2	–
J&J-51	3.5	−0.5	2.7	3.4	3.5	3.5	0.862	324.0	41.1	–
J&J-52	2.7	2.6	2.7	2.7	2.7	2.7	0.735	377.9	61.2	–
J&J-53	3.8	−3.1	0	2	2.9	3.8	0.724	472.0	75.6	–
J&J-54	4.6	−7.1	1.1	4.2	4.5	4.6	0.702	460.7	76.6	13.9
J&J-55	3.2	3.2	3.2	3.2	3.2	3.2	0.780	370.3	49.4	15.76
J&J-56	4.4	−0.9	2.3	4.1	4.3	4.4	0.744	359.5	57.3	12.97
J&J-57	3.5	−1.3	1.8	3.3	3.5	3.5	0.730	454.8	75.6	–
J&J-58	2.4	2.1	2.4	2.4	2.4	2.4	0.807	460.3	72.3	–
J&J-59	4.1	−2.8	0.3	2.3	3.2	4.1	0.710	457.0	66.4	–
J&J-60	2.9	2.8	2.9	2.9	2.9	2.9	0.731	456.0	83.5	–
J&J-61	3.7	3.6	3.7	3.7	3.7	3.7	0.745	437.6	85.0	–
J&J-62	5.0	−1.8	1.2	3.2	4.1	5	0.741	442.4	57.2	–
J&J-63	6.4	6.3	3.4	−0.5	−2.5	−6.7	0.709	495.8	100.9	3.21
J&J-64	2.9	−1.7	1.2	2.8	2.9	2.9	0.748	412.0	74.1	–
J&J-65	1.3	−3.3	1.1	1.3	1.3	1.3	0.820	326.5	73.8	–
J&J-66	5.3	−1.8	1.2	3.2	4.1	5.2	0.697	423.9	42.0	–
J&J-67	5.8	−1.1	1.9	3.9	4.9	5.7	0.785	450.5	54.4	–
J&J-68	2.5	2	2.5	2.5	2.5	2.5	0.739	427.5	81.4	13.65
J&J-69	5.6	−0.2	2.8	4.7	5.4	5.6	0.820	574.1	47.1	–
J&J-70	2.0	−4.4	−0.8	1.1	1.8	2	0.812	542.5	47.1	–

Table 4 (*Continued*)

J&J-71	4.8	−2	1	3	3.9	4.8	0.731	463.0	54.4	–
J&J-72	3.0	0.6	2.9	3	3	3	0.697	380.7	56.6	–
J&J-73	3.7	2.4	3.6	3.7	3.7	3.7	0.921	401.8	45.2	12.95
J&J-74	3.4	0.2	3.3	3.4	3.4	3.4	0.837	402.2	58.1	13.46
J&J-75	2.6	−2.1	0.9	2.4	2.6	2.6	0.818	280.7	41.1	–
J&J-76	2.0	−0.3	2	2	2	2	0.886	398.2	71.3	13.3
J&J-77	3.4	−1.3	1.6	3.2	3.4	3.4	0.741	429.3	74.1	–
J&J-78	3.3	−8.6	−2.7	−0.3	0.7	2.7	0.702	409.4	44.8	–
J&J-79	2.8	−3	−0.6	−0.5	−0.8	−2.5	0.760	366.0	40.5	2.3
J&J-80	2.7	−5.5	−1.9	0.1	1.1	2.6	0.745	383.0	61.9	–
J&J-81	3.8	−0.3	2.6	3.7	3.8	3.8	0.720	351.4	49.8	–
J&J-82	4.2	−3.4	0.2	2.2	3.2	4.1	0.787	284.7	61.4	–
J&J-83	2.6	−3.4	−0.9	−0.8	−1.1	−2.7	0.760	366.0	40.5	2.3
J&J-84	3.3	3.3	3.3	3.3	3.3	3.3	0.815	341.3	75.4	13.36
J&J-85	2.8	2.8	2.8	2.8	2.8	2.8	0.846	335.5	75.4	14.24
J&J-86	3.0	3	3	3	3	3	0.809	336.6	75.4	14.19
J&J-87	3.4	−8.5	−2.5	0.5	1.5	3.2	0.687	309.2	44.8	–
J&J-88	1.5	−5.8	−2.7	−0.7	0.3	1.5	0.773	389.2	97.1	14.02

tion. This analysis was performed using the PAMPA derived values of flux, P_{eff}, % retention, the calculated charge at pH 7.4 and the calculated physicochemical parameters as independent variables.

The fitting of a multiple linear regression model to describe an optimized relationship between LogBB and the calculated independent variables (without PAMPA data) resulted in the following equation:

$$\begin{aligned}\text{LogBB} = {} & 0.756 + 0.614 \times \text{CHARGE@pH 7.4} + 0.251 \\ & \times \text{Num\_H\_Acceptors} + 0.356 \times \text{Num\_H\_Donors} - 0.086 \\ & \times \text{Num\_RotatableBonds} - 0.415 \times \text{CMR} + 0.222 \times \text{CLOGP} \\ & - 0.032 \times \text{TPSA} + 0.009 \times \text{vdw\_area} \end{aligned} \quad (8)$$

Since the p-value in the ANOVA table is less than 0.05, there is a statistically significant relationship between the variables at the 95.0% confidence level. The adjusted R^2 value, which is more suitable for comparing models with different numbers of independent variables, indicates that the model explains 62.24% of the variability in LogBB. The predicted LogBB model is plotted against the observed LogBB values in Fig. 2.

By adding the PAMPA-BLM parameters (P_{eff}, flux and % retention) to the list of independent variables, the MLR with backward stepwise selection resulted in the following equation:

$$\begin{aligned}\text{LogBB} = {} & 0.392 + 0.0387 \times \text{PAMPA-BLM-}P_{\text{eff}}(10^{-6}\,\text{cm/s}) + 0.006 \\ & \times \text{PAMPA-BLM-\% Retention} + 0.537 \times \text{CHARGE@pH 7.4} \\ & + 0.142 \times \text{Num\_H\_Acceptors} + 0.347 \times \text{Num\_H\_Donors} \\ & - 0.077 \times \text{CMR} - 0.024 \times \text{TPSA} \end{aligned} \quad (9)$$

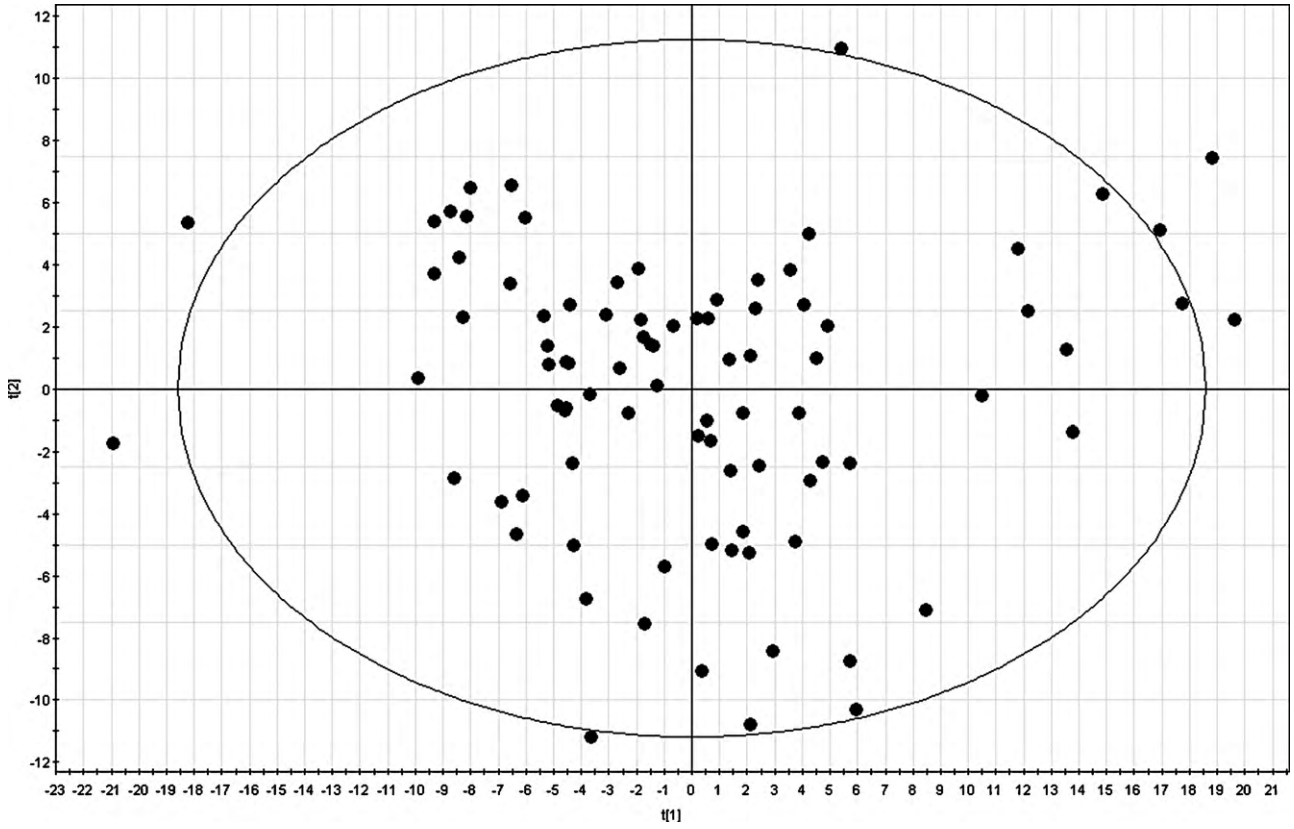

Fig. 1. Principal component analysis of the selected compounds with calculated and experimentally determined parameters. The PCA shows that most compounds are regularly distributed within the PCA-space (ellipse) resulting in a good representation of the entire dataset.

Table 5
Overview of the typical results of the partial least square (PLS) based models. *A*: number of principal components; *N*: number of J&J compounds; Remark: M1-4 – compounds described by the basic physicochemical properties and PAMPA results per assay separately; M5 – compounds described by the basic physicochemical properties without PAMPA results; M6-9 – compounds described by the basic physicochemical properties and MOE-descriptors together with results of PAMPA assays separately; M10 – compounds described by the basic physicochemical and MOE-descriptors together without any PAMPA results.

Model	Type	*A*	*N*	R^2	Q^2	Remark
M1	PLS	2	88	0.591	0.463	Physicochemical properties + BLM
M2	PLS	2	88	0.576	0.441	Physicochemical properties + DS
M3	PLS	2	88	0.597	0.479	Physicochemical properties + BBB
M4	PLS	2	88	0.523	0.393	Physicochemical properties + UWL
M5	PLS	2	88	0.520	0.395	Physicochemical properties
M6	PLS	3	88	0.770	0.609	MOE properties + BLM
M7	PLS	3	88	0.760	0.582	MOE properties + BBB
M8	PLS	3	88	0.761	0.585	MOE properties + DS
M9	PLS	3	88	0.774	0.635	MOE properties + UWL
M10	PLS	3	88	0.761	0.608	MOE properties

Table 6
J&J LogBBB data, in-vivo penetration classification, PAMPA-BLM and PAMPA-BBB P_{eff} values and bidirectional Caco-2 data of 27 structurally divers J&J compounds.

Compounds	Log BB	BBB class	PAMPA-BLM P_{eff} (10^{-6} cm/s)	PAMPA-BBB P_{eff} (10^{-6} cm/s)	Caco-2 AP-BL P_{app} (10^{-6} cm/s)	Caco-2 BL-AP P_{app} (10^{-6} cm/s)	Caco-2 efflux ratio
J&J-1	1.32	BBB+	13.61	29.45	20.1	36.7	1.8
J&J-4	−0.80	BBB−	4.66	10.68	14.5	30.8	2.1
J&J-7	−0.10	BBB−	0.04	12.07	2.8	21.97	7.8
J&J-8	1.04	BBB+	15.26	6.17	12.7	42.6	3.4
J&J-13	−1.10	BBB−	0.00	0.00	1.19	3.1	2.6
J&J-16	−0.42	BBB−	0.02	1.53	12.93	21.57	1.7
J&J-21	−2.00	BBB−	5.26	18.10	1.86	9.48	5.1
J&J-23	2.35	BBB+	35.15	15.34	48.4	61.3	1.3
J&J-29	0.87	BBB+	17.96	4.48	11.1	18	1.6
J&J-30	1.37	BBB+	17.67	8.61	13	24.9	1.9
J&J-36	1.32	BBB+	9.90	17.78	22.7	38.4	1.7
J&J-48	1.58	BBB+	13.36	6.94	93.7	22.8	0.2
J&J-51	1.20	BBB+	21.91	9.52	11.2	1.57	0.1
J&J-53	−0.22	BBB−	3.56	1.72	8.46	24.53	2.9
J&J-57	0.11	BBB+	14.01	5.22	133	38.2	0.3
J&J-58	−1.40	BBB−	0.48	4.34	4.7	57.57	12.2
J&J-59	−0.15	BBB−	12.37	3.13	13.86	48.1	3.5
J&J-60	−0.96	BBB−	1.06	3.66	26.87	40.17	1.5
J&J-61	−1.05	BBB−	3.27	12.30	152	41	0.3
J&J-62	0.68	BBB+	17.38	5.89	79	69.7	0.9
J&J-64	−1.00	BBB−	17.82	17.54	23.17	29.77	1.3
J&J-68	−1.22	BBB−	2.40	2.75	32.3	61	1.9
J&J-72	0.00	BBB+	21.20	8.53	170	53	0.3
J&J-75	1.08	BBB+	17.24	17.13	31.50	51.10	1.60
J&J-77	−1.22	BBB−	18.64	18.97	24.07	36.73	1.5
J&J-80	−0.70	BBB−	16.86	13.96	28.13	36.47	1.3
J&J-81	−0.15	BBB−	16.37	25.70	31.3	36.93	1.2

Table 7
Overview of 15 J&J compounds including plasma protein binding data.

Compounds	Log BB	Fraction unbound (rat) %	Log BB_u	PAMPA-BLM P_{eff} (10^{-6} cm/s)	PAMPA-DS P_{eff} (10^{-6} cm/s)	PAMPA-BBB P_{eff} (10^{-6} cm/s)	PAMPA-BBB-UWL P_{eff} (10^{-6} cm/s)
J&J-11	−0.35	3.50	1.11	14.31	2.28	0.00	28.49
J&J-19	−0.62	65.40	−0.44	0.76	66.84	5.99	0.31
J&J-26	−1.00	12.70	−0.10	3.54	51.34	6.25	90.51
J&J-29	0.87	7.30	2.00	17.96	46.56	4.48	35.22
J&J-30	1.37	9.00	2.42	17.67	30.72	8.61	358.52
J&J-34	0.28	34.20	0.73	3.89	91.07	9.32	1.99
J&J-35	−1.00	1.20	0.81	12.15	29.63	12.82	93.73
J&J-42	−0.52	0.80	1.68	9.92	36.50	13.38	23.39
J&J-47	0.70	8.90	1.75	13.62	53.18	3.84	22.40
J&J-51	1.20	22.60	1.84	21.91	63.73	9.52	20.47
J&J-65	−1.00	5.70	0.22	3.22	57.28	8.45	11.09
J&J-69	0.30	3.70	1.67	8.74	64.27	–	105.89
J&J-70	−0.30	26.40	0.27	3.03	55.37	12.73	60.83
J&J-75	1.08	23.90	1.86	17.24	46.84	17.13	35.61
J&J-88	−0.60	63.30	−0.45	0.01	47.96	3.75	7.82

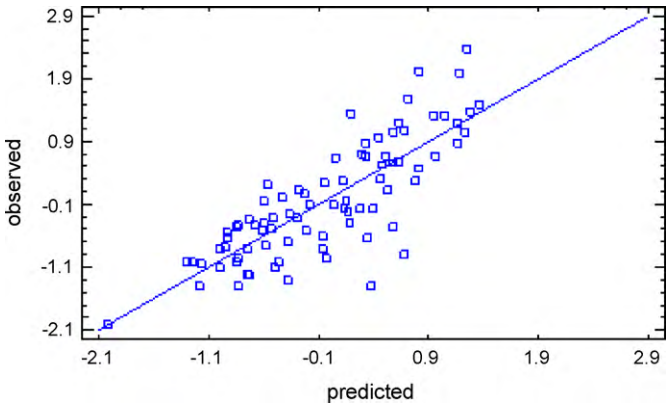

Fig. 2. Observed LogBB values versus predicted LogBB values. The predicted LogBB data are obtained by multiple linear regression (MLR) with backward stepwise selection of the parameters including the calculated physicochemical properties only.

with the p-value <0.05 showing a statistically significant relationship between the variables at the 95.0% confidence level. For this equation, the adjusted R^2 value is 70.27%. Although the coefficients of the PAMPA parameters (P_{eff} and % retention) are small, the model explains more of the variability in LogBB compared to the model without PAMPA-BLM. The predicted LogBB model is plotted against the observed LogBB values in Fig. 3. Evaluation of the parameters of the other PAMPA-models in the set of independent variables did not result in an improved model to predict LogBB.

3.6. Combination of Caco-2 efflux and PAMPA data to predict the BBB classification

In a previous study (Mensch et al., 2010), the PAMPA-BLM model as well as the PAMPA-BBB model predicted the passive diffusion of a subset of compounds reasonably well based on the classification ranges that were established for both models using commercially available compounds (training set). The false positive values obtained, could be explained by their action as substrates for active efflux. In this study, a larger set of 27 compounds were evaluated in a bidirectional Caco-2 assay to determine the efflux ratio (Table 6). These compounds were selected based on their diversity in LogBB values, chemical structures and physicochemical properties. Because the PAMPA-BBB-UWL, PAMPA-DS and the Caco-2 permeability results did not discriminate between the BBB+ and the BBB− compounds, the efflux values in this work were combined with only the PAMPA-BLM and PAMPA-BBB data. Based on the BBB+ and BBB− discrimination limits for both the PAMPA-BLM and the PAMPA-BBB models, obtained by Mensch et al. (2010), the P_{eff} were plotted against the LogBB values for these compounds (Figs. 4 and 5).

For the 27 compounds, the PAMPA-BLM model misclassified 10 compounds, all categorized as false positives. The obtained efflux ratios of four false positive outliers showed moderate efflux tendencies (efflux ratio > 2) which suggests that misclassification could be

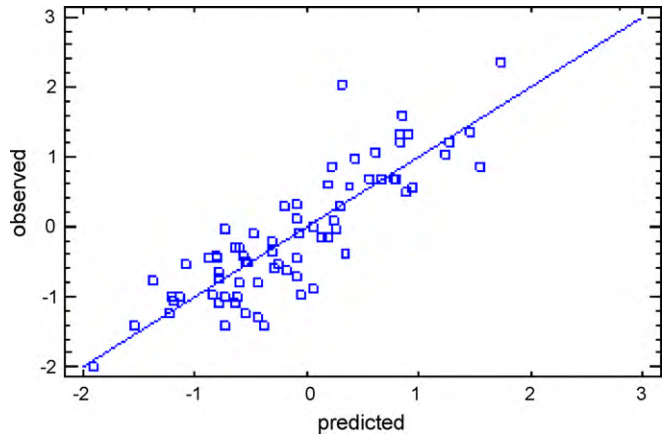

Fig. 3. Observed LogBB values versus predicted LogBB values. The predicted LogBB data are obtained by MLR with backward stepwise selection of the parameters including the calculated physicochemical properties PAMPA-BLM parameters (P_{eff}, flux and % retention).

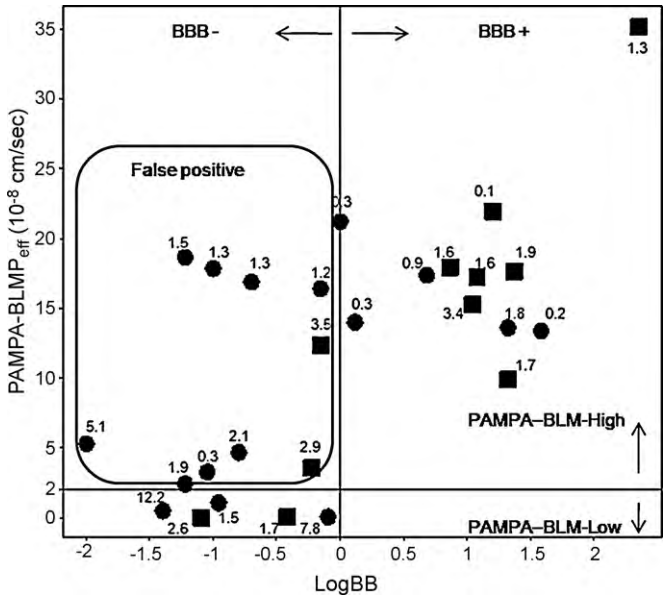

Fig. 4. PAMPA-BLM P_{eff} values plotted versus LogBB of 27 compounds. Efflux ratios are stated at the data points. ● are data obtained after subcutaneous administration while ■ are obtained after oral dosing. The earlier determined classification limit (2×10^{-6} cm/s) for the PAMPA-BLM model separates the high BBB permeable compounds from the low BBB permeable compounds (Mensch et al., 2009).

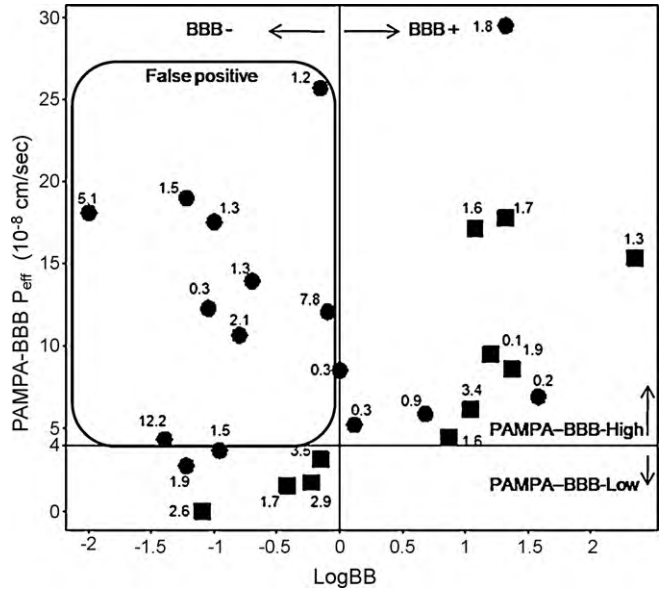

Fig. 5. PAMPA-BBB P_{eff} values plotted versus LogBB of 27 compounds. Efflux ratios are stated at the data points. ● are data obtained after subcutaneous administration while ■ are obtained after oral dosing. The earlier determined classification limit (4×10^{-6} cm/s) for the PAMPA-BBB model separates the high BBB permeable compounds from the low BBB permeable compounds (Mensch et al., 2009).

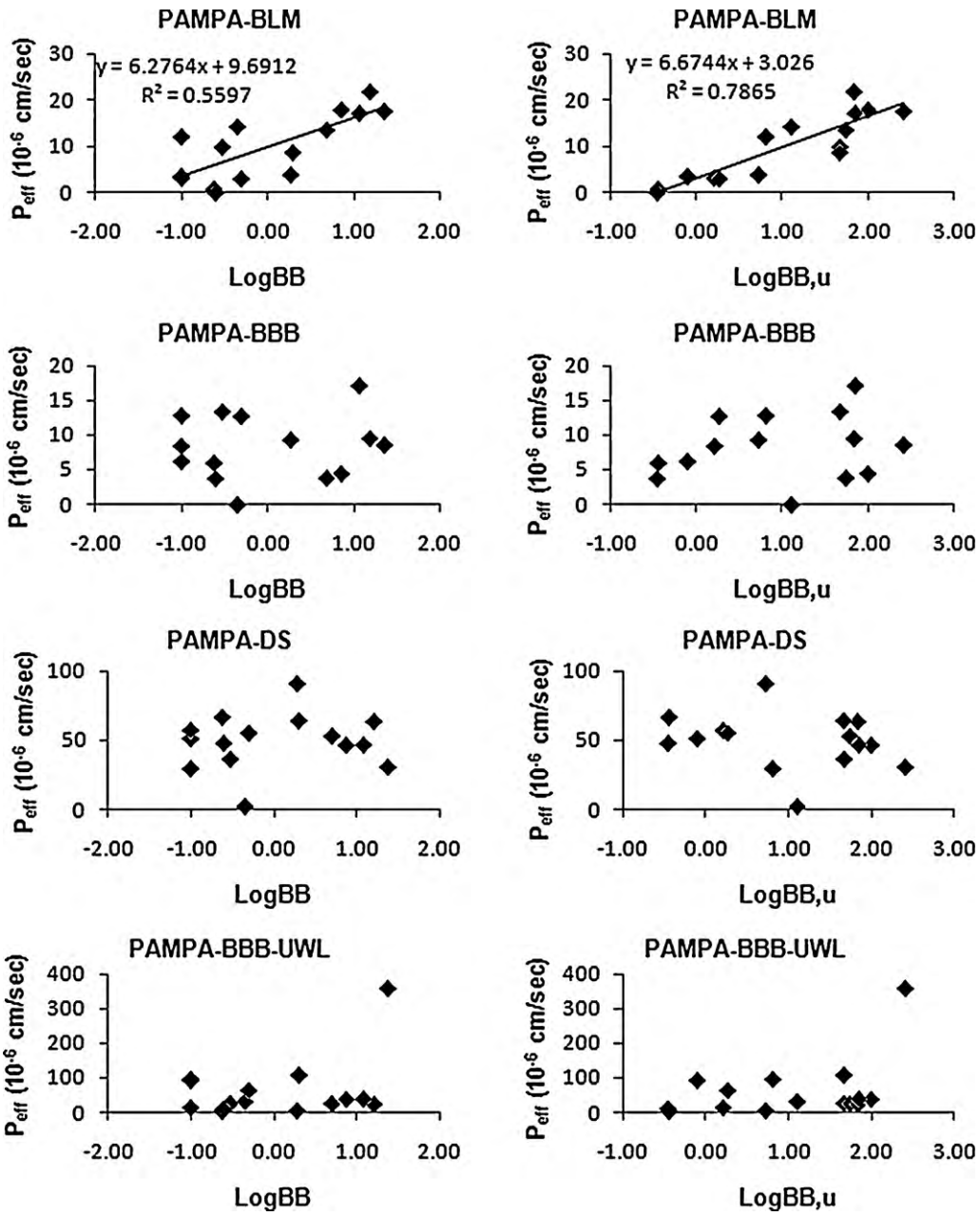

Fig. 6. Obtained PAMPA-P_{eff} values for 15 J&J compounds obtained by all PAMPA-models are plotted versus the LogBB (left-hand side) and versus $LogBB_u$ (right-hand side). The combination of the P_{eff}, obtained with PAMPA-BLM, and plasma protein binding, results in an improved correlation with LogBB. Integration of PPB data with parameters of the other PAMPA-models does not improve the releation with LogBB.

attributed to the effect of P-gp related efflux. Nevertheless, six compounds (J&J 61, 64, 68, 77, 80± and 81) with an efflux ratio smaller than 2 remain misclassified.

The PAMPA-BBB model classified 11 J&J compounds correctly as BBB+ and 6 J&J compounds as BBB− (Fig. 5). Nine compounds appeared to manifest a false positive outcome of which four compounds were shown to be substrates for moderate efflux as a result of which five compounds (J&J 61, 64, 77, 80 and 81) were classified as false positive outliers. These results demonstrate that P_{eff} values, obtained from PAMPA-BLM as well as PAMPA-BBB, combined with Caco-2 efflux data are useful to classify early discovery compounds in BBB+ or BBB− classes. However, ±20% of the compounds are classified as false positive outliers.

3.7. Influence of plasma protein binding on the prediction of LogBB

To evaluate the influence of PPB on the prediction of LogBB, 15 chemically diverse compounds, comprising a broad range of LogBB values, were tested in a dialysis experiment with rat plasma. The obtained fraction unbound (f_u) values are reported in Table 7 together with the resulting calculated $LogBB_u$ and all PAMPA-P_{eff} results. The influence of fraction unbound in plasma on the predictability of the PAMPA-models is shown in Fig. 6. No useful relationships between the P_{eff} of the PAMPA-models (BBB, DS and BBB-UWL) and LogBB as well as $LogBB_u$ is established. However, a weak correlation

between the P_{eff} of the PAMPA-BLM model and LogBB can be observed ($R^2 = 0.56$). This correlation is improved by taking into account the fractions unbound in the rat plasma ($R^2 = 0.79$). These results indicate that the free fraction of drug in the plasma can play an important role in predicting the extent of CNS penetration observed in-vivo using the original PAMPA-BLM model.

4. Conclusions

Partial least square analysis as well as multiple linear regression with backward stepwise selection of variables are interesting statistical tools to investigate correlations between dependent and independent variables. Both methodologies, obtain comparable outcomes in the prediction of LogBB from calculated as well as experimentally obtained compound properties albeit using different statistical approaches. Both methodologies show that the contribution of the PAMPA parameters in the prediction of LogBB is limited.

Apart from that, the analysis showed that the models containing the PAMPA-BLM parameters perform better compared with the other PAMPA models evaluated in this study. These findings are confirmed when the free fraction of drug in the plasma is taken into account which allows the transformation of LogBB values in $LogBB_u$. Only the effective permeability from the PAMPA-BLM model was shown to have an improved relationship with $LogBB_u$.

Despite these results, it should be emphasized that PAMPA is used as a screening tool in drug discovery, ideally to determine the permeability classification of molecules as soon as possible. In this context, both the PAMPA-BLM model, a traditional paradigm for the prediction of GI absorption, and the PAMPA-BBB model similarly predicted the LogBB classification of the J&J compounds based on the classification ranges that were established for both models (Mensch et al., 2010). Misclassifications with both models could be classified as false positives. Part of the false positive misclassifications could be attributed to the compounds being substrates for active efflux. On the other hand, ±20% of the 27 tested compounds remained misclassified even taking the efflux status into account.

Besides PAMPA, plasma protein binding experiments and bidirectional Caco-2 assays are often used in high throughput assessments in early discovery programs. An integrated approach of all three aforementioned in-vitro methodologies can possibly guide the discovery scientist to improved prediction of brain penetration. However, it is important to recognize that simplistic in-vitro models cannot represent the complicated distribution in the human brain.

Acknowledgments

The authors wish to thank Koen Wuyts and the ADME-tox in-vivo group for providing the in-vivo LogBB data. Thanks to Chantal Masungi, Pascale Dehertogh and Marleen Van Dooren and An Tuytelaers for their support in the Caco-2 assessment and LC/MS/MS analysis.

References

Abbott, N.J., 2002. Astrocyte-endothelial interactions and blood-brain barrier permeability. J. Anat. 200, 629–638.
Abbott, N.J., 2005. Dynamics of CNS barriers: evolution, differentiation and modulation. Cell Mol. Neurobiol. 25, 5–23.
Abbott, N.J., Rönnbäck, L., Hansson, E., 2006. Astrocyte-endothelial interactions at the blood-brain barrier. Nat. Rev. Neurosci. 7, 41–53.
Abraham, M.H., 2004. The factors that influence permeation across the blood-brain barrier. Eur. J. Med. Chem. 39, 235–240.
Abraham M.H., Hersey A., 2006. In: Testa, B., van de Waterbeemd, H. (Eds.), Comprehensive Medicinal Chemistry, 2nd ed., vol. 5. ADMET/Property-based approaches.
Abraham, M.H., Ibrahim, A., Zhao, Y.H., Acree Jr., W.E., 2006b. A data base for partition of volatile organic compounds and drugs from blood/plasma/serum to brain, and an LFER analysis of the data. J. Pharm. Sci. 95, 2091–2100.
Avdeef, A., 2003a. Absorption and Drug Development; Solubility, Permeability and the Charged State. John Wiley & Sons, Inc., New Jersey, pp. 116–246.
Avdeef, A., 2003b. High throughput measurements of permeability profiles. In: van de Waterbeemd, H., Lennernäs, H., Artursson, P. (Eds.), Drug Bioavailibility, Estimation of Solubility, Permeability, Absorption and Bioavailability. Wiley–VCH, Weinheim, pp. 46–71.
Avdeef, A., 2005. The rise of PAMPA. Expert Opin. Drug Metab. Toxicol. 1, 325–342.
Avdeef, A., Bendels, S., Di, L., Faller, B., Kansy, M., Sugano, K., 2007. PAMPA – critical factors for better predictions of absorption. J. Pharm. Sci. 96, 2893–2909.
Begley, D., Brightman, M.W., 2003. Structural and functional aspects of the blood-brain barrier. Prog. Drug Res. 61, 40–78.
Bentz, J., Tran, T.T., Polli, J.W., Ayrton, A., Ellens, H., 2005. The steady-state Michaelis–Menten analysis of P-glycoprotein mediated transport through a confluent cell monolayer cannot predict the correct Michaelis constant Km. Pharm. Res. 22, 1667–1677.
Brewster, M.E., Noppe, M., Peeters, J., Loftsson, T., 2007. Effect of the unstirred water layer on permeability enhancement by hydrophilic cyclodextrins. Int. J. Pharm. 342, 250–253.
Brightman, M.W., Reese, T.S., 1969. Junctions between intimately apposed cell membranes in the vertebrate brain. J. Cell Biol. 40, 648–677.
Brownson, E.A., Abbruscato, T.J., Gillespie, T.J., Hruby, V.J., Davis, T.P., 1994. Effect of peptidases at the blood brain barrier on the permeability of enkephalin. J. Pharmacol. Exp. Ther. 270, 675–680.
Cisternino, S., Mercier, C., Bourasset, F., Rouse, F., Scherrmann, J.M., 2004. Expression, upregulation, and tranport activity of the multidrug-resistance protein Abcg2 at the mouse blood brain barrier. Cancer Res. 64, 3296–3301.
Clark, D.E., 1999. Rapid calculation of polar molecular surface area and its application to the prediction of transport phenomena. 2. Prediction of blood-brain barrier penetration. J. Pharm. Sci. 88, 815–821.
Di, L., Kerns, E.H., Fan, K., McConnell, O.J., Carter, G.T., 2003. High throughput artificial membrane permeability assay for the blood brain barrier. Eur. J. Med. Chem. 38, 223–232.
Ecker, G.F., Noe, C.R., 2006. In-silico prediction models for blood-brain barrier permeation. In: Dermietzel, R., Spray, D.C., Nedergaard, M. (Eds.), Blood-Brain Barriers: from Ontogeny to Artificial Interfaces, vol. 1. Wiley-VCH Verlag GmbH & Co.KGaA, Weinheim, Germany, pp. 403–428.
Hammarlund-Udenaes, M., Fridén, M., Syvänen, S., Gupta, A., 2008. On the rate and extent of drug delivery to the brain. Pharm. Res. 25, 1737–1750.
Hitchcock, S.A., Pennington, L.D., 2006. Structure-brain exposure relationships. J. Med. Chem. 49, 7559–7583.
Instruction Manual for PAMPA Evolution Permeability Analyzer, 2004. Version 2.2.0, pION Inc.
Jeffrey, P., Summerfield, S.G., 2007. Challenges for blood-brain barrier (BBB) screening. Xenobiotica 3, 1135–1151.
Kansy, M., Senner, F., Gubernator, K., 1998. Physicochemical high throughput screening: parallel artificial membrane permeation assay in the description of passive absorption processes. J. Med. Chem. 41, 1007–1010.
Kerns, E.H., Di, L., Petusky, S., Farris, M., Ley, R., Jupp, P., 2004. Combined application of parallel artificial membrane permeability assay and Caco-2 permeability assays in drug discovery. J. Pharm. Sci. 93, 1440–1453.
Konovalov, D.A., Coomans, D., Deconinck, E., Vanderheyden, Y., 2007. Benchmarking of QSAR models for blood-brain barrier permeation. J. Chem. Inf. Model. 47, 1648–1656.
Krämer, S.D., Abbott, N.J., Begley, D.J., 2001. Biological models to study blood-brain barrier permeation. In: Testa, B., van de Waterbeemd, H., Folkers, G., Guy, R. (Eds.), Pharmacokinetic Optimization in Drug Research: Biological, Physicochemical and Computational Strategies. Wiley-VCH, Weinheim, pp. 127–153.
Lipinski, C.A., 2004. Lead- and drug-like compounds: the rule-of-five revolution. Drug Discov. Today Technol. 1, 337–341.
Masungi, C., Mensch, J., Van Dijck, A., Borremans, C., Willems, B., Mackie, C., Noppe, M., Brewster, M.E., 2008. Parallel artificial membrane permeability assay(PAMPA) combine with a 10-day cell culture as a tool for assessing new drug candidates. Pharmazie 63, 194–199.
Maurer, T.S., DeBartolo, D.B., Tess, D.A., Scott, D.O., 2005. Relationship between exposure and nonspecific binding of thirty-three central nervous system drugs in mice. Drug Metab. Dispos. 33, 175–181.
McIntosh, A.R., Bookstein, F.L., Haxby, J.V., Grady, C.L., 1996. Spatial pattern analysis of functional brain images using partial least squares. NeuroImage 3, 143–157.
Mensch, J., Melis, A., Mackie, C., Verreck, G., Brewster, M.E., Augustijns, P., 2010. Evaluation of various PAMPA models to identify the most discriminating method for the prediction of BBB permeability. Eur. J. Pharm. Biopharm. 74, 495–502.
Mensch, J., Noppe, M., Adriaensen, J., Melis, A., Mackie, C., Augustijns, P., Brewster, M.E., 2006. Novel generic UPLC/MS/MS method for high throughput analysis applied to permeability assessment in early drug discovery. J. Chrom. B 847, 182–187.
Pardridge, W.M., 1991. Peptide Drug Delivery to the Brain. Raven Press, New York, pp. 52–88.
Pardridge, W.M., 1995. Transport of small molecules through the blood-brain barrier: biology and methodology. Adv. Drug. Deliv. 15, 5–36.
Reese, T.S., Karnovsky, M.J., 1967. Fine structural localization of a blood-brain barrier to exogenous peroxidase. J. Cell Biol. 34, 207–217.
Rose, K., Hall, L., Kier, L.B., 2002. Modeling blood-brain barrier partitioning using electrotopological state. J. Chem. Inf. Comput. Sci. 42, 651–666.

Sugano, K., Takata, N., Machida, M., Saitoh, K., Terada, K., 2002. Prediction of passive intestinal absorption using biomimetic artificial membrane permeation assay and the parallel pathway model. Int. J. Pham. 241, 241–251.
Summerfield, S.G., Stevens, A.J., Cutler, L., del Carmen Osuna, M., Hammond, B., Tang, S.T., Hersey, A., Spalding, D.J., Jeffrey, P., 2006. Improving the in-vitro prediction of in-vivo CNS penetration: integrating permeability, Pgp efflux and free fractions in blood and brain. J. Pharmacol. Exp. Ther. 316, 1282–1290.
Sun, H., 2004. A universal molecular descriptor system for prediction of LogP, LogS, LogBB, and absorption. J. Chem. Inf. Comput. Sci. 44, 748–757.
Urbano-Cuadrado, M., Luque-Ruiz, I., Gómez-Nieto, M.A., 2007. QSAR models based on isomorphic and nonisomorphic data fusion for predicting the blood brain barrier permeability. J. Comput. Chem. 28, 1252–1260.
van de Waterbeemd, H., Gifford, E., 2003. ADMET in-silico modelling: towards prediction paradise? Nat. Rev. Drug Discov. 2, 192–204.
van de Waterbeemd, H., Camenisch, G., Folkers, G., Chretien, J.R., Raevsky, O.A., 1998. Estimation of blood-brain barrier crossing of drugs using molecular size and shape, and H-bonding descriptors. J. Drug Target. 6, 151–165.
Wichmann, K., Diedenhofen, M., Klamt, A., 2007. Prediction of blood-brain partitioning and human serum albumin binding based on COSMO-RS σ-moments. J. Chem. Inf. Model. 47, 228–233.
Wold, S., Sjöström, M., Eriksson, L., 2001. PLS-regression: a basic tool of chemometrics. J. Chemometrics 58, 109–130.